Quantum well interband semiconductor lasers highly tolerant to dislocations

Laurent Cerutti, Daniel A Díaz Thomas, Jean-Baptiste Rodriguez, Marta Rio Calvo, Gilles Patriarche, A. N. Baranov, Eric Tournié

Research Article Vol. 8, No. 11 / November 2021 / Optica 1397

OPTICA

Quantum well interband semiconductor lasers highly tolerant to dislocations

Laurent Cerutti,[1,*] Daniel A. Díaz Thomas,[1] Jean-Baptiste Rodriguez,[1] Marta Rio Calvo,[1] Gilles Patriarche,[2] Alexei N. Baranov,[1] and Eric Tournié[1]

[1]IES, Univ. Montpellier, CNRS, F-34000 Montpellier, France
[2]C2N, CNRS-Univ. Paris-Sud, Univ. Paris-Saclay, 10 Avenue Thomas Gobert, F-91120 Palaiseau, France
*Corresponding author: laurent.cerutti@umontpellier.fr

Received 2 August 2021; accepted 6 September 2021 (Doc. ID 438272); published 2 November 2021

III-V semiconductor lasers integrated on Si-based photonic platforms are eagerly awaited by the industry for mass-scale applications, from interconnect to on-chip sensing. The current understanding is that only quantum dot lasers can reasonably operate at the high dislocation densities generated by the III-V-on-Si heteroepitaxy, which induces high non-radiative carrier recombination rates. Here we propose a strategy based on a type-II band alignment to fabricate quantum well lasers highly tolerant to dislocations. A mid-IR GaInSb/InAs interband cascade laser grown on Si exhibits performances similar to those of its counterpart grown on the native GaSb substrate, in spite of a dislocation density in the 10^8 cm^{-2} range. Over 3800 h of continuous-wave operation data have been collected, giving an extrapolated mean time to failure exceeding 312,000 h. This validates the proposed strategy and opens the way to new integrated laser development.

https://doi.org/10.1364/OPTICA.438272

1. INTRODUCTION

Integration of semiconductor lasers onto Si substrates has attracted considerable attention to combine the many possible photonic functions with the advantages of well-established silicon technology. Different strategies have thus been investigated in view of integrating semiconductor lasers onto Si substrates. An attractive approach to address this problem consists of using lasers based on quasi-direct-bandgap group-IV materials such as highly doped-Ge [1] or GeSn [2,3], but despite important efforts, adequate laser performances are still confined to low temperature or to optical pumping, and their integration remains a great challenge. Up to now, highly efficient and robust direct bandgap III-V semiconductors have remained the most promising materials for the integration of coherent light sources onto silicon substrates. For 20 years, the integration of III-V semiconductors on Si has thus been intensively investigated to develop on-chip light sources in silicon photonics with high yield and cost reduction. The most mature technologies are based on heterogeneous integration such as wafer bonding [4,5], regrowth on bonded templates [6], or transfer printing [7]. Heterogeneous integration can be a viable solution, but the high cost of the native substrate and the complex processing must be first addressed before a transfer to industrial production. On the other hand, direct epitaxial integration is the most promising approach to provide high volume capability [8], but it is still challenging because of the formation of defects inherent to the III-V heteroepitaxy on Si, namely, threading dislocations (TDs) and antiphase boundaries (APBs). The propagation of APBs related to the growth of polar III-Vs on on-axis non-polar Si substrates can be suppressed through careful growth strategies leading to their annihilation [9–14]. The high density of TDs, arising from the large lattice mismatch between III-V semiconductors (besides GaP) and Si, remains thus the main obstacle to the demonstration of high performance and reliable devices. Nevertheless, rapid performance and reliability improvement of lasers directly grown on Si was recently obtained with InAs/GaAs quantum dot (QD) lasers grown on silicon [15,16]. Extrapolated lifetimes ranging from 1000 up to 30,000,000 h were estimated for TD density of 5×10^8 down to 7×10^6 cm^{-2}, respectively, due to complex buffer layers [17,18] between the Si substrate and the laser structure. These results show that QD lasers [19,20] are sensitive to TDs at densities larger than 10^7 cm^{-2}. As for conventional quantum well (QW) lasers, they are even more sensitive [21,22] with lifetimes around 200 h [23,24] for TD density of 5×10^7 cm^{-2}.

2. CONCEPT FOR ACTIVE REGIONS HIGHLY TOLERANT TO DISLOCATIONS

The drastic degradation of the threshold current and laser lifetime with the TD density is associated with non-radiative trap levels created by the TDs, which are typically represented as discrete energy levels within the energy bandgap. In such a configuration, these defect-related traps act as recombination channels that drastically reduce the carrier population available for radiative recombination and thus degrade the overall laser performances. The determination of the position of the trap levels related to defects in general and dislocations in particular is a challenge.

In the absence of experimental data, we have located the trap levels at mid-gap, where they operate as the most efficient non-radiative centers. This configuration is commonly used in the literature to represent the dislocation-related non-radiative recombination centers in III-V lasers grown on Si [22,25,26]. Figure 1(a) illustrates schematically the band diagram of a type-I QW and the various competing carrier recombination paths in the presence of dislocations. The non-radiative process promotes the motion and generation of dislocations through recombination-enhanced defect reaction (REDR) and limits the device lifetime [25,26]. The superior tolerance to TDs of QD over QW lasers is related to the carrier localization within the QDs, which reduces their interaction with the defects located in the layers surrounding the QDs [22,26]. Still, long-lived QD lasers require low TD densities to drastically reduce non-radiative recombination in the whole structure.

From this observation, two important points must be addressed when designing the active region to overcome the performance sensitivity of interband QW lasers to TDs. First, non-radiative recombination in the layers around the QWs should be eliminated/mitigated. This can be achieved by inserting carrier blocking layers on both sides of the QWs to prevent the electrons (holes) from escaping to the *p*-side (*n*-side) of the structure. Second, the radiative recombination path should not cross the non-radiative trap levels, which can be achieved by engineering the band alignment of the QW/barrier pair. For instance, QWs employing a type-II/III heterostructure, where the electrons and holes are confined in adjacent materials, allow independent tuning of the conduction and valence band edges through careful materials selection, which, in turn, makes it possible to adjust the relative positions of the radiative transition and trap levels. Figure 1(b) illustrates a type-II structure that satisfies this strategy. In this configuration, non-radiative recombination through the trap levels has little efficiency, and the active region becomes highly tolerant to defects.

The requirements necessary to realize such a design are met, for example, in the active region of the Sb-based type-II QW interband cascade laser (ICL) [27]. These lasers have become the most efficient interband optical source for the MIR spectral range (spanning the 3–6 μm wavelength range). ICLs operating in continuous wave (CW) at temperatures higher than 100°C [28] are now commercially available but only on expensive and small sized GaSb and InAs substrates [29,30], which prevents their wide use in diverse commercial applications such as trace gas analysis or control of industrial processing [31]. Figure 1(c) represents typical energy band profiles for one period of an ICL active region. The interband radiative transition occurs in a "W" type-II QW [32] composed of a GaInSb hole QW sandwiched between two InAs electron QWs. The "W" QW is surrounded by hole and electron injectors composed of a series of alternating and graded thickness GaSb/AlSb and InAs/AlSb layers, respectively. These layers provide injection of the carriers into the active QW. Also, these materials prevent the electron (hole) from escaping in the hole (electron) injector and thus act as blocking layers, suppressing non-radiative recombination around the QWs. Then, to stack QWs, this configuration requires electrons in the valence band tunnel to the conduction band through a semi-metallic interface (SMIF) to be injected in the next active region.

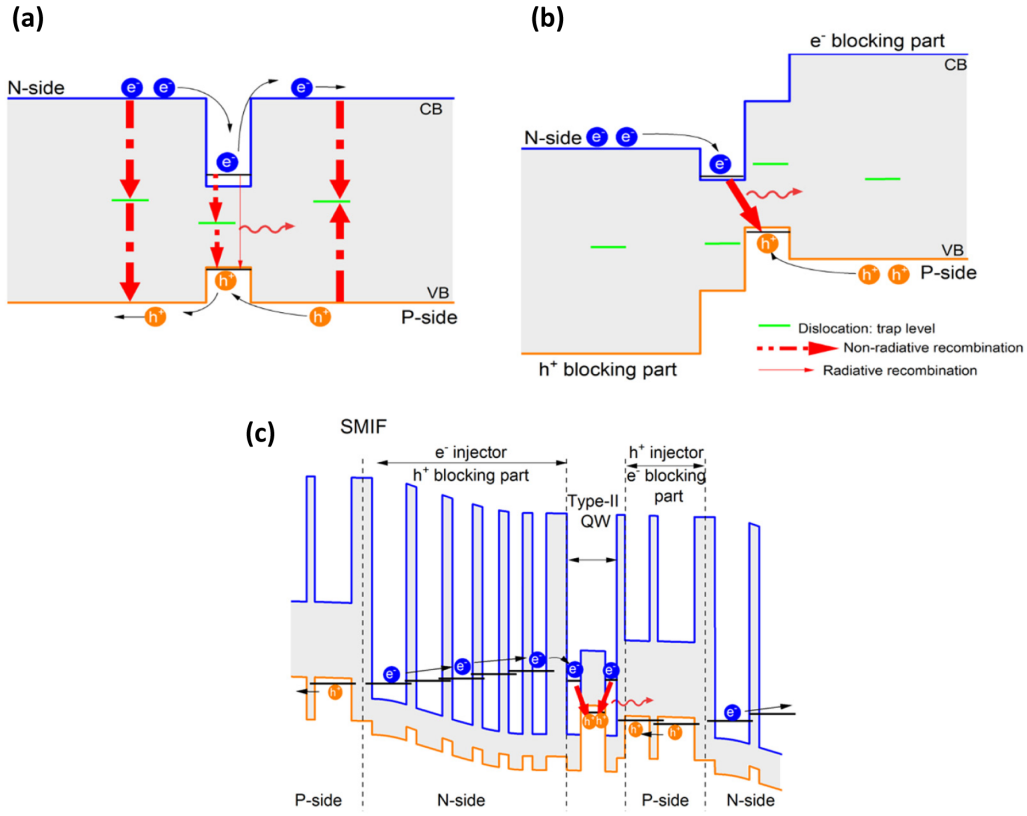

Fig. 1. (a) Representation of the recombination processes in a type-I QW active region and (b) in a type-II QW active region with electron and hole blocking parts. Injected carriers may relax via non-radiative recombination through defect centers introduced by TDs or radiative recombination within the QW. In (a), carrier can recombine non-radiatively, while in (b), non-radiative recombinations are suppressed. (c) Type-II QW ICL with band diagram criteria represented in (b).

3. GROWTH AND STRUCTURAL CHARACTERIZATIONS OF ICL ON SILICON SUBSTRATE

In this work, a type-II ICL structure was directly grown by solid source molecular beam epitaxy (SS-MBE) on an on-axis Si (001) substrate. The ∼12% lattice mismatch between GaSb and Si results in a high density of dislocations (∼10^{13} cm^{-2}) at the interface. First a 1.5 μm thick GaSb-on-Si buffer layer was grown. The laser structure consisted of seven IC stages designed for emission at 3.5 μm surrounded by a GaSb separate confinement heterostructure (SCH) and *N*-type AlSb/InAs superlattice cladding layers (see Supplement 1 Section 1 for details). The total thickness of the structure is around 7.9 μm, below the 10 μm thickness where cracks appear in GaSb-based laser grown on Si [33].

Figure 2 shows cross-sectional transmission electronic microscope (TEM) images of the ICL structure grown on the Si substrate. The seven active stages are perfectly visible, and Fig. 2(c) shows the good agreement between the real structure and the targeted thicknesses. Most of the dislocations generated at the GaSb/Si interface are confined within the first 500 nm, while some propagate into the whole structure [Fig. 2(a)]. The density at the top of the GaSb buffer is in the 8−9.10^8 cm^{-2} range, and despite the AlSb/InAs superlattice cladding, a high density (∼5.10^8 cm^{-2}) of TDs is still present in the QW active region [Figs. 2(a) and 2(b)].

The ICL structure was then processed (see Supplement 1 Section 1 for details) into 8 μm wide ridges with both contacts taken on the epitaxial structure. One contact was formed on top of the ridge and another one in the AlSb/InAs bottom cladding layer as illustrated in the Fig. 3. The processed structure without facet coating was cleaved into devices with various cavity lengths.

4. MEASUREMENTS AND RESULTS

Figure 4(a) shows typical light-current-voltage (L-I-V) curves measured in CW at 20°C for cavity lengths of 1, 2, and 3 mm. The I-V curves exhibit a turn-on voltage of 3 V, which is comparable to our similar ICLs grown on GaSb processed in the same way and operating in the same wavelength range (see Supplement 1 Section 2 for details). The I-V curves show a soft turn-on, also seen on ICLs grown on GaSb and processed using a BCl_3 dry etching chemistry [34]. However, the series resistances are in the range of 20–30 ohms for 3 to 1 mm cavity lengths, respectively. We attribute this unexpectedly high value, in comparison to the 1–3 ohms obtained for ICLs grown on GaSb, to the lateral current path and the poor electrical conductivity of the low-doped upper part of the AlSb/InAs bottom cladding layer where this contact is located. This behavior has already been observed when the contact is taken in the AlSb/InAs cladding layer [34]. The laser threshold current ranges from 30 to 70 mA, depending on the cavity length. These values are close to those of our ICLs grown on GaSb substrates. The output power reaches 19 mW per uncoated facet for the 2–3 mm long cavities. The slope efficiency (per facet) varies from 0.22 to 0.3 W/A, depending on the cavity length, while the external differential quantum efficiency (related to the two facets), defined as

$$\eta_d = \frac{q}{h\nu}\frac{dP}{dI},$$

with q the electron charge, h the Planck's constant, and ν the frequency of light, ranges between 124% and 170%, values comparable to ICLs grown on GaSb.

Figure 4(b) presents the evolution of the emission spectra of the 2 mm long ICL under various CW injection currents at 20°C. At 35 mA, the spectrum exhibits a broad band of spontaneous emission with a maximum at 3.425 μm and a full width half maximum (FWHM) of 172 nm. Above threshold, laser action starts at the long-wavelength side of the spontaneous spectrum at 3.436 μm.

In addition, the thermal performance was also assessed. The L-I characteristics at different temperatures displayed in Fig. 5(c) demonstrate that CW lasing was maintained up to 50°C. The threshold current is temperature dependent and increases from 39 to 106 mA between 15°C and 50°C. Thus, the characteristic temperature [Fig. 5(a) inset] that represents the sensitivity of the threshold current to the device temperature is 43 K between 15°C

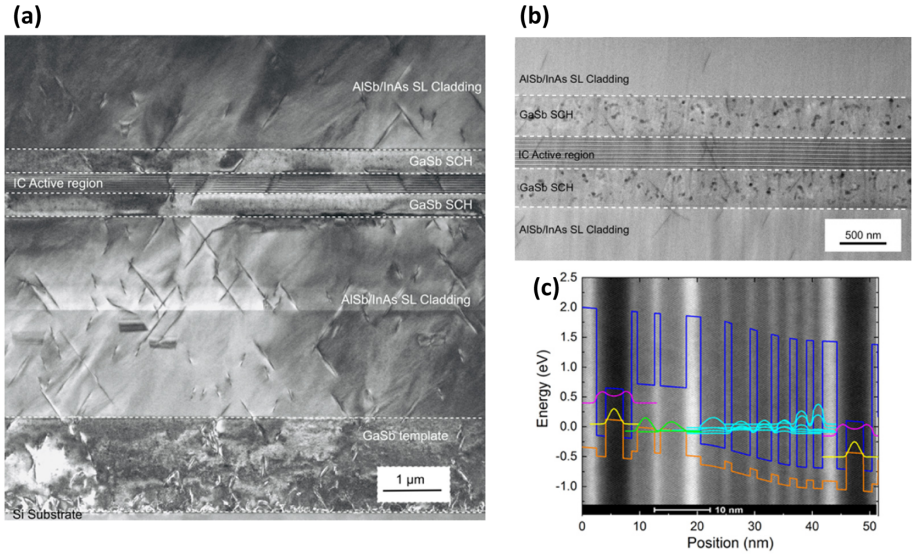

Fig. 2. Cross-sectional TEM images of the ICL directly grown on Si. (a) CCD image of the whole structure revealing the defects. (b) Bright field scanning transmission electronic microscope (STEM) image of the ICL active region. (c) Simulated band diagram (methods) and probability density functions for an internal electric field of 80 kV/cm of one stage of the ICL active region overlaid on top of the bright field STEM image. The probability densities for the active electron (hole) are indicated with magenta (yellow) lines, while those for the injector- electron (hole) are indicated with cyan (green) lines.

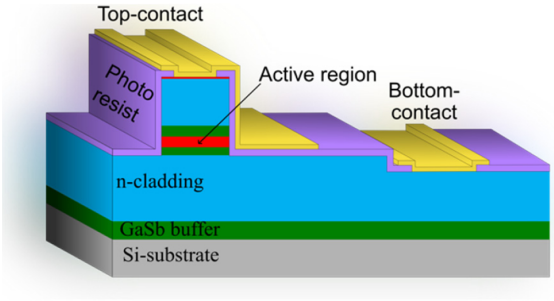

Fig. 3. Schematic representation of the processed ICL grown on Si substrate.

and 35°C and 26 K between 40°C and 50°C, which is comparable to the characteristic temperature of ICLs grown on GaSb. The emission spectra at different temperatures are plotted in Fig. 5(d). They reveal multimode operation and a peak emission wavelength increasing from 3.49 μm at 15°C to 3.53 μm at 45°C.

Thus, despite the high density of dislocations, these ICLs grown on Si present performances comparable to those of similar devices grown on GaSb. Nevertheless, the route for a viable commercialization of III-V lasers directly integrated on Si requires adequate uniformity of device performances and long operating lifetime. The L-I curves of 15 as-cleaved devices selected along the radius of the wafer are presented in Fig. 6(a). The important point is that all lasers are working, and the histogram of the corresponding threshold current [inset Fig. 6(a)] shows that it fluctuates between 43 and 47 mA, even if a couple of devices present lower performances related to imperfect facet cleavage and device processing (see Supplement 1 Section 3 for details). Aging of the laser at high temperature under CW operation demonstrates high long-term reliability and stability, important parameters for their use in real life without a thermo-electric cooling system. An ICL grown on Si was aged at 40°C under CW operation at a constant applied current of 120 mA (∼1.5 times the threshold current) while periodic L-I measurements around the threshold were also performed to track changes [inset Fig. 6(a)].

Figure 6(b) shows the aging trends of the laser power and threshold current. The ICL grown on Si presents an increase of 2.8% of the threshold current and a reduction of output power of 6.5% after 3800 h operation in CW at 40°C. The mean time to failure (MTTF), defined as the time required for doubling the initial threshold current, is then extrapolated to over 312,000 h (see Supplement 1 Section 4 for details).

To our knowledge, it is the first report of a lifetime longer than 1000 h for any interband (QW or QD) laser with a density of dislocations above 10^8 cm^{-2}. Indeed, the QD lasers proposed as the best solution for the direct growth of lasers on Si suffer a lifetime limited to ∼1000 h at these TD densities [35], and require complex buffer layers to lower the dislocation density and thus improve their performances.

In this work, the proposed design is insensitive to a TD density in the range of 10^8 cm^{-2} and tackle the main issues concerning the realization of III-V interband lasers grown on Si, namely, nonradiative recombination and REDR and approach the long lifetime obtained on ICL grown on GaSb [36].

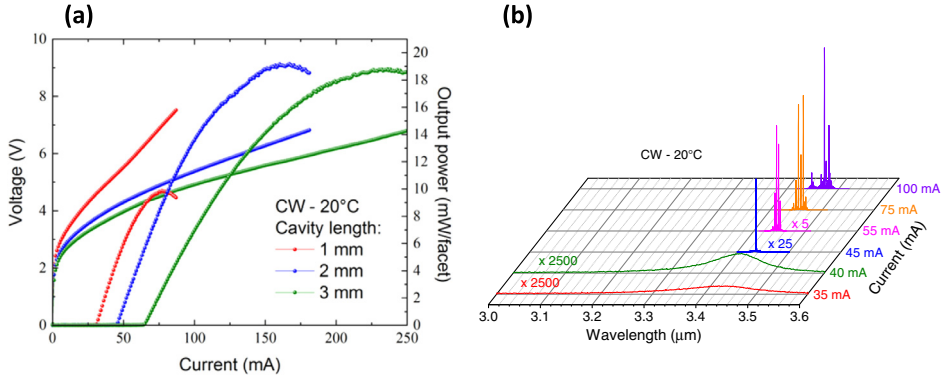

Fig. 4. CW performances of ICL grown on Si. (a) L-I-V characteristics at 20°C for 8 μm wide ridge and various cavity lengths. (b) Emission spectra for an 8 μm × 2 mm laser at different injection currents.

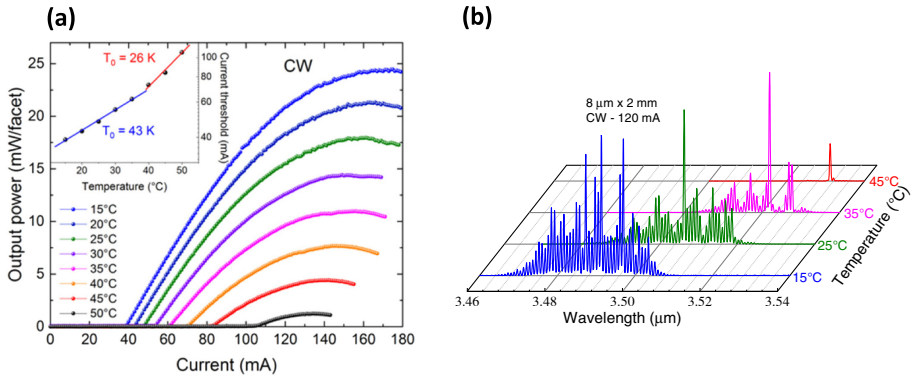

Fig. 5. CW performances of an 8 μm × 2 mm ICL grown on Si at various temperatures. (a) L-I-V characteristics. Inset: semi-logarithmic variation of the current threshold with temperature. (b) Emission spectra.

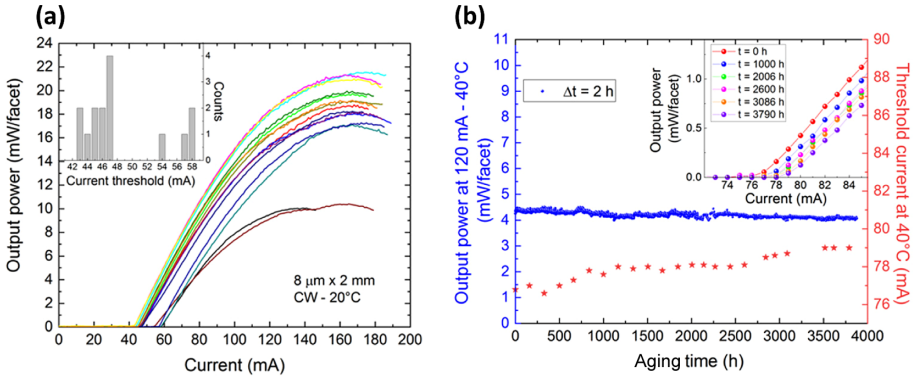

Fig. 6. CW reliability of ICL grown on silicon. (a) L-I characteristics of the 15 8 µm × 2 mm ICLs tested at 20°C. Inset: histogram of CW threshold current at 20°C. (b) Aging data at 40°C and under 120 mA current injection. Inset: L-I characteristics of the laser around the threshold at different times of aging.

5. CONCLUSION

In conclusion, a highly defect-tolerant interband QW laser grown on (001) Si was demonstrated. This unprecedented result has been achieved due to the design of the active region of a type-II QW GaSb-based ICL that allowed mitigating non-radiative recombination through dislocation-related trap levels. Despite a TD density higher than 10^8 cm^{-2}, CW operation was achieved up to 50°C with a threshold current around 45 mA and output power per facet of 20 mW at 20°C. We expect that these performances can be further improved through reduction of series resistance and the use of facet coating. Moreover, the aging test showed very slow degradation after 3800 h of CW operation at 40°C, which allowed to extract a minimum MTTF of 312,000 h in these conditions. The obtained results open the door for low-cost production of high-performance MIR lasers on large-sized Si substrates and also MIR photonic sensors on Si-photonic integrated circuits (PIC) [37]. Finally, this approach could be adapted to other compound semiconductor families, such as InP [38], GaAs [39], or ZnSe [40], where type-II QWs present similarity to our concept. This would allow covering a large wavelength range with QW lasers highly tolerant to dislocations.

Funding. Agence Nationale de la Recherche (ANR-11-EQPX-0016, ANR-16-CE24-0011).

Acknowledgment. We thank the French RENATECH network for FIB preparation and TEM measurement.

Disclosures. L.C, J.B.R, A.N.B, and E.T. filed a FR provisional patent (no. 2107138) based on the results reported in this paper (P). The remaining authors declare no competing interests.

Data availability. Data underlying the results presented in this paper are not publicly available at this time but may be obtained from the authors upon reasonable request.

Supplemental document. See Supplement 1 for supporting content.

REFERENCES

1. J. Liu, X. Sun, R. Camacho-Aguilera, L. C. Kimerling, and J. Michel, "Ge-on-Si laser operating at room temperature," Opt. Lett. **35**, 679–681 (2010).
2. S. Wirths, R. Geiger, N. Von Den Driesch, G. Mussler, T. Stoica, S. Mantl, Z. Ikonic, M. Luysberg, S. Chiussi, J. M. Hartmann, H. Sigg, J. Faist, D. Buca, and D. Grützmacher, "Lasing in direct-bandgap GeSn alloy grown on Si," Nat. Photonics **9**, 88–92 (2015).
3. A. Elbaz, D. Buca, N. von den Driesch, K. Pantzas, G. Patriarche, N. Zerounian, E. Herth, X. Checoury, S. Sauvage, I. Sagnes, A. Foti, R. Ossikovski, J. M. Hartmann, F. Boeuf, Z. Ikonic, P. Boucaud, D. Grützmacher, and M. El Kurdi, "Ultra-low-threshold continuous-wave and pulsed lasing in tensile-strained GeSn alloys," Nat. Photonics **14**, 375–382 (2020).
4. L. Liu, R. Kumar, K. Huybrechts, T. Spuesens, G. Roelkens, E. J. Geluk, T. De Vries, P. Regreny, D. Van Thourhout, R. Baets, and G. Morthier, "An ultra-small, low-power, all-optical flip-flop memory on a silicon chip," Nat. Photonics **4**, 182–187 (2010).
5. G. Crosnier, D. Sanchez, S. Bouchoule, P. Monnier, G. Beaudoin, I. Sagnes, R. Raj, and F. Raineri, "Hybrid indium phosphide-on-silicon nanolaser diode," Nat. Photonics **11**, 297–300 (2017).
6. Y. Hu, D. Liang, K. Mukherjee, Y. Li, C. Zhang, G. Kurczveil, X. Huang, and R. G. Beausoleil, "III/V-on-Si MQW lasers by using a novel photonic integration method of regrowth on a bonding template," Light Sci. Appl. **8**, 93 (2019).
7. J. Justice, C. Bower, M. Meitl, M. B. Mooney, M. A. Gubbins, and B. Corbett, "Wafer-scale integration of group III-V lasers on silicon using transfer printing of epitaxial layers," Nat. Photonics **6**, 610–614 (2012).
8. A. Y. Liu and J. Bowers, "Photonic integration with epitaxial III-V on silicon," IEEE J. Sel. Top. Quantum Electron. **24**, 6000412 (2018).
9. Y. Wan, J. Norman, Q. Li, M. J. Kennedy, D. Liang, C. Zhang, D. Huang, Z. Zhang, A. Y. Liu, A. Torres, D. Jung, A. C. Gossard, E. L. Hu, K. M. Lau, and J. E. Bowers, "13 µm submilliamp threshold quantum dot micro-lasers on Si," Optica **4**, 940–944 (2017).
10. J. Kwoen, B. Jang, J. Lee, T. Kageyama, K. Watanabe, and Y. Arakawa, "All MBE grown InAs/GaAs quantum dot lasers on on-axis Si (001)," Opt. Express **26**, 11568–11576 (2018).
11. C. Shang, A. C. Gossard, J. E. Bowers, Y. Wan, J. C. Norman, N. Collins, I. MacFarlane, M. Dumont, S. Liu, Q. Li, and K. M. Lau, "Low-threshold epitaxially grown 1.3 µm InAs quantum dot lasers on patterned (001) Si," IEEE J. Sel. Top. Quantum Electron. **25**, 1–7 (2019).
12. L. Monge-Bartolome, T. Cerba, D. A. Díaz-Thomas, M. Bahriz, M. R. Calvo, G. Boissier, T. Baron, J.-B. Rodriguez, L. Cerutti, and E. Tournié, "Etched-cavity GaSb laser diodes on a MOVPE GaSb-on-Si template," Opt. Express **28**, 20785–20793 (2020).
13. M. Rio Calvo, L. Monge Bartolomé, M. Bahriz, G. Boissier, L. Cerutti, J.-B. Rodriguez, and E. Tournié, "Mid-infrared laser diodes epitaxially grown on on-axis (001) silicon," Optica **7**, 263–266 (2020).
14. K. Li, J. Yang, Y. Lu, M. Tang, P. Jurczak, Z. Liu, X. Yu, J. Park, H. Deng, H. Jia, M. Dang, A. M. Sanchez, R. Beanland, W. Li, X. Han, J. Zhang, H. Wang, F. Liu, S. Chen, A. Seeds, P. Smowton, and H. Liu, "Inversion boundary annihilation in GaAs monolithically grown on on-axis silicon (001)," Adv. Opt. Mater. **8**, 2000970 (2020).
15. S. Chen, W. Li, J. Wu, Q. Jiang, M. Tang, S. Shutts, S. N. Elliott, A. Sobiesierski, A. J. Seeds, I. Ross, P. M. Smowton, and H. Liu, "Electrically pumped continuous-wave III–V quantum dot lasers on silicon," Nat. Photonics **10**, 307–311 (2016).

16. D. Jung, Z. Zhang, J. Norman, R. Herrick, M. J. Kennedy, P. Patel, K. Turnlund, C. Jan, Y. Wan, A. C. Gossard, and J. E. Bowers, "Highly reliable low-threshold InAs quantum dot lasers on on-axis (001) Si with 87% injection efficiency," ACS Photon. **5**, 1094–1100 (2018).
17. M. Tang, S. Chen, J. Wu, Q. Jiang, K. Kennedy, P. Jurczak, M. Liao, R. Beanland, A. Seeds, and H. Liu, "Optimizations of defect filter layers for 1.3-μm InAs/GaAs quantum-dot lasers monolithically grown on Si substrates," IEEE J. Sel. Top. Quantum Electron. **22**, 50–56 (2016).
18. D. Jung, P. G. Callahan, B. Shin, K. Mukherjee, A. C. Gossard, and J. E. Bowers, "Low threading dislocation density GaAs growth on on-axis GaP/Si (001)," J. Appl. Phys. **122**, 225703 (2017).
19. J. Selvidge, E. T. Hughes, J. C. Norman, C. Shang, M. J. Kennedy, M. Dumont, A. M. Netherton, Z. Zhang, R. W. Herrick, J. E. Bowers, and K. Mukherjee, "Reduced dislocation growth leads to long lifetime InAs quantum dot lasers on silicon at high temperatures," Appl. Phys. Lett. **118**, 192101 (2021).
20. C. Shang, E. Hughes, Y. Wan, M. Dumont, R. Koscica, J. Selvidge, R. Herrick, A. C. Gossard, K. Mukherjee, and J. E. Bowers, "High-temperature reliable quantum-dot lasers on Si with misfit and threading dislocation filters," Optica **8**, 749–754 (2021).
21. A. Y. Liu, S. Srinivasan, J. Norman, A. C. Gossard, and J. E. Bowers, "Quantum dot lasers for silicon photonics," Photon. Res. **3**, B1–B9 (2015).
22. Z. Liu, M. Martin, T. Baron, S. Chen, A. Seeds, R. Penty, I. White, H. Liu, C. Hantschmann, M. Tang, Y. Lu, J.-S. Park, M. Liao, S. Pan, A. Sanchez, and R. Beanland, "Origin of defect tolerance in InAs/GaAs quantum dot lasers grown on silicon," J. Lightwave Technol. **38**, 240–248 (2020).
23. Z. I. Kazi, P. Thilakan, T. Egawa, M. Umeno, and T. Jimbo, "Realization of GaAs/AlGaAs lasers on Si substrates using epitaxial lateral overgrowth by metalorganic chemical vapor deposition," Jpn. J. Appl. Phys. **40**, 4903–4906 (2001).
24. B. Shi, S. Pinna, H. Zhao, S. Zhu, and J. Klamkin, "Lasing characteristics and reliability of 1550 nm laser diodes monolithically grown on silicon," Phys. Status Solidi **218**, 2000374 (2021).
25. A. Y. Liu, R. W. Herrick, O. Ueda, P. M. Petroff, A. C. Gossard, and J. E. Bowers, "Reliability of InAs/GaAs quantum dot lasers epitaxially grown on silicon," IEEE J. Sel. Top. Quantum Electron. **21**, 690–697 (2015).
26. M. Buffolo, F. Samparisi, C. De Santi, D. Jung, J. Norman, J. E. Bowers, R. W. Herrick, G. Meneghesso, E. Zanoni, and M. Meneghini, "Physical origin of the optical degradation of InAs quantum dot lasers," IEEE J. Quantum Electron. **55**, 1–7 (2019).
27. R. Q. Yang, "Infrared laser based on intersubband transitions in quantum wells," Superlattices Microstruct. **17**, 77–83 (1995).
28. I. Vurgaftman, W. W. Bewley, C. L. Canedy, C. S. Kim, M. Kim, C. D. Merritt, J. Abell, J. R. Lindle, and J. R. Meyer, "Rebalancing of internally generated carriers for mid-infrared interband cascade lasers with very low power consumption," Nat. Commun. **2**, 585 (2011).
29. I. Vurgaftman, R. Weih, M. Kamp, J. R. Meyer, C. L. Canedy, C. S. Kim, M. Kim, W. W. Bewley, C. D. Merritt, J. Abell, and S. Höfling, "Interband cascade lasers," J. Phys. D **48**, 123001 (2015).
30. J. Meyer, W. Bewley, C. Canedy, C. Kim, M. Kim, C. Merritt, and I. Vurgaftman, "The interband cascade laser," Photonics **7**, 75 (2020).
31. E. Tournié and L. Cerutti, *Mid-Infrared Optoelectronics* (Elsevier, 2020).
32. J. R. Meyer, C. A. Hoffman, F. J. Bartoli, and L. R. Ram-Mohan, "Type-II quantum-well lasers for the mid-wavelength infrared," Appl. Phys. Lett. **67**, 757 (1995).
33. L. Monge-Bartolome, B. Shi, B. Lai, G. Boissier, L. Cerutti, J.-B. Rodriguez, K. M. Lau, and E. Tournié, "GaSb-based laser diodes grown on MOCVD GaAs-on-Si templates," Opt. Express **29**, 11268–11276 (2021).
34. A. Spott, E. J. Stanton, A. Torres, M. L. Davenport, C. L. Canedy, I. Vurgaftman, M. Kim, C. S. Kim, C. D. Merritt, W. W. Bewley, J. R. Meyer, and J. E. Bowers, "Interband cascade laser on silicon," Optica **5**, 996–1005 (2018).
35. D. Jung, R. Herrick, J. Norman, K. Turnlund, C. Jan, K. Feng, A. C. Gossard, and J. E. Bowers, "Impact of threading dislocation density on the lifetime of InAs quantum dot lasers on Si," Appl. Phys. Lett. **112**, 153507 (2018).
36. I. E. Trofimov, C. L. Canedy, C. S. Kim, M. Kim, W. W. Bewley, C. L. Merritt, I. Vurgaftman, J. R. Meyer, and L. T. Le, "Interband cascade lasers with long lifetimes," Appl. Opt. **54**, 9441–9445 (2015).
37. H. Lin, Z. Luo, T. Gu, L. C. Kimerling, K. Wada, A. Agarwal, and J. Hu, "Mid-infrared integrated photonics on silicon: a perspective," Nanophotonics **7**, 393–420 (2017).
38. S. Sprengel, A. Andrejew, K. Vizbaras, T. Gruendl, K. Geiger, G. Boehm, C. Grasse, and M.-C. Amann, "Type-II InP-based lasers emitting at 2.55 μm," Appl. Phys. Lett. **100**, 041109 (2012).
39. D. A. Duffy, I. P. Marko, C. Fuchs, T. D. Eales, J. Lehr, W. Stolz, and S. J. Sweeney, "Performance characteristics of low threshold current 1.25 μm type-II GaInAs/GaAsSb 'W'-lasers for optical communications," J. Phys. D **54**, 365104 (2021).
40. J. C. Banthí-Barcenas, F. Sutara, and I. Hernández-Calderón, "Growth and characterization of type I quantum wells based on ZnCdSe/ZnTe Type II heterostructures confined within ZnSe barriers," J. Electron. Mater. **47**, 4399–4403 (2018).